Journal of Materials and Electronic Devices 2 (2025) 20-25

JOURNAL OF MATERIALS AND ELECTRONIC DEVICES

JMED

Optical properties of MXene-based hybrid nanocomposites

Kadir DEMIRELLI*

Faculty of Science, Department of Chemistry, University of Firat, 23169 Elazig, Turkey

$Ti_3C_2T_x$ MXene/PANI (polyaniline), $Ti_3C_2T_x$ MXene0.19/PbO and MXene0.03/PbO0.86/ PANI0.11 nanocomposites were synthesized by in situ polymerisation with lead(II)oxide (PbO) nanoparticles produced via hydrothermal route. The fundamental scientific and future development trends and research directions of MXene-based organic and inorganic nanocomposites in the field of optical functional materials are anticipated. The structural and optical properties of $Ti_3C_2T_x$ MXene0.19/PbO and MXene0.03/PbO0.86/PANI0.11 nanocomposites were examined, including absorbance (A), reflectance (R), optical band gap (E_{op}), Urbach energy (E_u), refractive index (n), the real part of the complex dielectric permittivity (ε′) and optical conductivity (σ′). The absorbance spectra revealed maximum absorption peaks at 636 nm for $Ti_3C_2T_x$ MXene0.19/PbO and 332 nm for MXene0.03/PbO0.86/ PANI0.11.

Keywords: *Optic characterization, MXene, PbO, PANI, nanocomposite*.

Submission Date: 03 August 2025
Acceptance Date 15 November 2025

**Corresponding author: kdemirelli@firat.edu.tr*

1. Introduction

Transition metal carbides/nitrides/carbonitrides, known as MXenes, exhibit tremendous potential for optical applications due to their diverse elemental compositions and tunable structural properties [1–3]. This review, which is based on the synthesis methods and optical characteristics of MXenes, focuses on recent advancements in MXene-based optical functional materials and analyzes the performance enhancement mechanisms of MXene-based materials for photothermal conversion and photocatalysis. The fundamental scientific and technological challenges in the field of MXene-based optical functional materials are outlined, and future development trends and research directions for MXene-based optical materials are projected. Recently, the photoactive semiconductor material PbO has attracted extensive research interest due to its efficient use in paints, sensor applications, and pigments [4,5]. PbO polymorphs have become a major subject of investigation in optical applications and have exhibited various structural behaviors [6–9]. Polymers are rarely used in their pure form in product development; they are typically reinforced with nanoparticles/additives/fibers to improve their mechanical and optical properties. Hybrid polymer nanocomposites, such as PP1PbS/CdS [10], also exhibit enhanced mechanical and optical characteristics. To produce elastomer nanocomposites, elastomers reinforced with silica nanoparticles, LS, carbon black, and CNTs have been utilized [11, 12]. In order to improve the mechanical behavior of thermoset polymers and prepare thermoset nanocomposites for various applications, organic or inorganic additives—such as clay, diamond, graphite, alumina, and oxides—have been incorporated [13]. Critical parameters in the interfacial region formed between polymers and nanoparticles include particle size distribution, interfacial interactions, processing methods, and the melting temperature of the nanoparticles, among others.

This study was designed based on the preparation of nanostructured composite thin films consisting of PANI and a PbO matrix incorporated with the 2D transition metal

$Ti_3C_2T_x$ for optical applications. The synthesized PbO-based nanocomposites were aimed to be investigated in terms of their optical properties using UV–Visible spectroscopy. By performing absorbance (A) and reflectance (R) measurements with an optical characterization system, the band gaps of the nanocomposites were determined.

2. Experimental

2.1. Materials and analytical techniques

Commercially purchased aniline was purified by vacuum distillation prior to its use in the polymerization process. Ammonium persulfate (APS, Merck) was used as received as the oxidizing agent. Lead(II) acetate trihydrate [$Pb(CH_3COO)_2 \cdot 3H_2O$] and sodium hydroxide (NaOH), supplied by Merck (USA), were employed as precursor materials in the synthesis of PbO nanoparticles. Ti_3AlC_2 MAX phase (particle size ≤ 100 nm) and hydrofluoric acid (ρ = 1.15 g/mL, 48% HF solution) were also obtained from Merck. SEM measurements were performed with BAUM ZEISS Sigma 300 FESEM (Field Emission Scanning Electron Microscope). The optical characterization system was used to measure reflectance (R) and absorbance (A).

2.2. Hydrothermal synthesis of Ti_3C_2Tx MXene/PANI nanocomposite

The MXene/PANI nanocomposite was synthesized according to the procedure described in the literature [18]. For this purpose, ANI was converted into PANI through a redox reaction in the presence of $Ti_3C_2T_x$ MXene. An autoclave was loaded with 0.11 g of $Ti_3C_2T_x$ MXene and 0.25 g of $(NH_4)_2S_2O_7$, followed by the addition of approximately 30 mL of deionized water. After adding an aqueous 1.0 M HCl solution to the mixture, sonication was applied for 15 minutes. The autoclave was then placed in a hydrothermal system and kept at 180 °C for 24 hours. The resulting $Ti_3C_2T_x$ MXene/PANI nanocomposite dispersion was precipitated at 3000 rpm. After removing the supernatant, the remaining nearly black powder particles were washed with distilled water, and the dispersion was again precipitated at 3000 rpm. This procedure was repeated two more times. Afterwards, the powdered solid phase was dried under vacuum at 60 °C for 24 hours.

2.3. Hydrothermal synthesis of $Ti_3C_2T_x$ MXene:PANI:PbO

Following the methodology reported in the literature, the $Ti_3C_2T_x$ MXene0.03:PANI0.11:PbO0.86 nanocomposite was synthesized using the MXene0.19:PANI nanocomposite prepared in Section 2.2 [14]. In this process, PbO was generated in situ via a hydrothermal autoclave reaction in the presence of $Ti_3C_2T_x$ MXene0.19:PANI to produce $Ti_3C_2T_x$ MXene0.03: PANI0.11:PbO0.86 nanocomposite. Initially, 0.80 g of $Pb(CH_3COO)_2 \cdot 3H_2O$ was dissolved in 10 mL of deionized water in a beaker and subjected to sonication for 20 minutes. Subsequently, 10 mL of an aqueous solution containing 0.20 g of NaOH was added, followed by an additional 10 minutes of sonication to ensure complete dispersion and reaction. In a separate beaker, 0.2 g of the MXene/PANI nanocomposite obtained in Section 2.1 was dispersed in 10 mL of distilled water and sonicated for 1 minute. The two dispersions were then combined in a Teflon-lined autoclave and subjected to hydrothermal treatment at 180 °C for 24 hours. After cooling to room temperature, the resulting mixture was processed according to the procedure described in Section 2.2, yielding blackish powder-like particles corresponding to the $Ti_3C_2T_x$ MXene0.03:PANI0.11:PbO:0.86 nanocomposite.

3. Results and Discussion

Given that *Ti_3C_2Tx* MXenes are considered a class of metamaterials, their optical characteristics—as well as their energy bandgap, direct or indirect transition behavior, and topological features—are intrinsically governed by their underlying electronic structure. The electronic structure of MXenes, which endows them with a wide range of multifunctional properties, is highly sensitive to several factors, including the type and density of surface terminal groups, chemical composition, crystal symmetry, dimensionality, applied electric field, doping level, and the presence of localized electronic states [15–17]. Consequently, accurately resolving the energy-level architecture and associated optical responses of specific MXene systems remains a considerable challenge, often requiring advanced computational and spectroscopic approaches. Most of MXenes exhibit either metallic conductivity or behave as narrow-bandgap semiconductors. Such electronic characteristics primarily originate from their distinctive crystal structures and the significant contribution of the outer transition-metal d-orbital electrons. These d-orbital electrons play a critical role in shaping the energy band structure and, consequently, govern the overall electronic behavior of MXene materials [18-20]. From that perspective, it is more meaningful to determine the band gap of MXenes, which are metal oxides or nanocomposites prepared with organic materials. SEM images of MXene0.19:PANI were recorded in th Fig. 1. The SEM images of the MXene0.19:PANI nanocomposite were recorded at different magnifications: 5 μm (20,000×), 2 μm (50,000×), and 1μm (100,000×). In all three SEM images, both the matrix (PANI) and the MXene particles can be observed within the composite system. However, in Fig. 1c, which was taken at 100,000× magnification, the PANI fibers and the MXene layers are visualized more clearly.

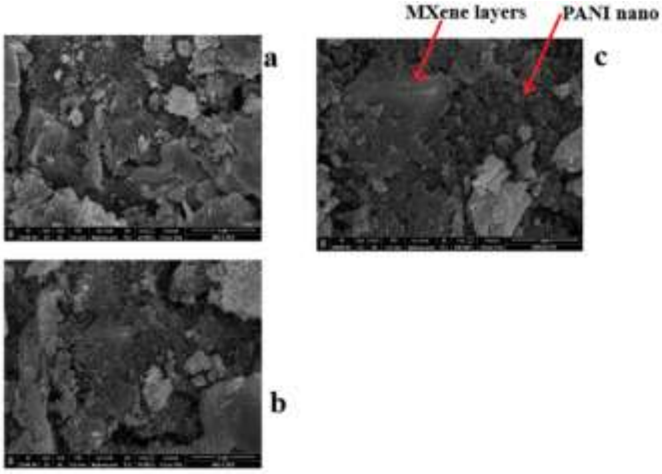

Fig.1. SEM images magnitudes of a) 5µm b) 2µm c) 1µm for MXene0.19:PANI nanocomposite

3.1. Optical Properties of Nanocomposites

The characterization of optical properties using UV–visible absorption spectroscopy is widely employed to investigate the optical behavior of various inorganic and organic nanoparticles. The absorbance characteristics of hybrid nanomaterials typically depend on several factors, including band gap, impurity centers, oxygen vacancies, and surface roughness. The UV–visible measurements of the MXene0.19:PANI and MXene0.03:PANI0.11: PbO0.86 nanocomposites were carried out in the 200–800 nm range, and the absorbance data were recorded as a function of wavelength (Fig. 2a and 2b). The UV–visible spectra of the nanocomposites exhibit a single and distinct absorption peak. In this regards, The MXene0.19–PANI nanocomposite exhibited a maximum absorption peak at 333 nm, whereas the MXene0.03:PANI0.11:PbO0.86 nanocomposite showed a maximum absorption band at 636 nm. The refractance spectra of MXene0.19/PANI and the MXene0.03:PANI0.11:PbO0.86 nanocomposite was recorded in the range 200-800 nm. The refrectance values as a function of wavelength were plotted as seen in Fig. 3a and 3b, respectively. The optical band gap of a material can be calculated by the following equation 1 (Eq. 1).

$$(\alpha h\nu)=A(h\nu-Eg)^{n} \quad (1)$$

where, n is a constant indicating the type of optical transition and indicates the allowed direct transition when n is equal to 1/2 and the allowed indirect transitions when n is equal to 2. Direct and indirect transitions indicate optical transitions in semiconductor materials. It is well known that there is a direct transition along the band gap between the valence and conduction band edges in K space and that the total energy and momentum of the electron-photon system must be conserved during the transition. Fig. 4a and 4b showed the graphs of $(\alpha h\nu)^2$ versus photon energy. Fig. 4a shows that the band gap of MXene0.19/PANI is 1.5 eV, while that of the ternary composite (Fig. 4b) is 2.14 eV. Thus, the incorporation of MXene and PANI can effectively alter the surface morphology of the PbO matrix film, leading to variations in its optical properties. In the literature, the band gap of undoped PbO thin films is reported to be 2.59 eV. For doped PbO films, the optical band gap has been reported to vary between 2.72 and 1.66 eV, depending on the Mn doping concentration [21]. Additionally, Mn-doped PbO thin films exhibit a clearly observable wavelength-dependent oscillatory behavior in refractive index and dielectric constants. In this study, the band gap of the MXene0.03:PANI0.11:PbO0.86 nanocomposite was determined to be 2.14 eV (Fig. 4b). The slightly lower band gap value compared to pure PbO is attributed to the presence of MXene and PANI within the composite system, both of which exhibit enhanced electrical conductivity. MXenes exhibit excellent light-absorption properties across the entire solar spectrum. The band gap of a material determines the photon energies it can absorb [22]. When the photon energy exceeds the forbidden energy gap of the material, the transition of electrons from the valence band to the conduction band becomes easier, thereby enabling the material to absorb light at that energy [23]. In this context, MXenes generally possess a relatively small band gap and can therefore absorb a broad range of photon energies [24]. Thus, it is understood that the band gap of MXene0.19:PANI, determined as 1.5 eV from the graph in Fig. 4a, is an expected value.

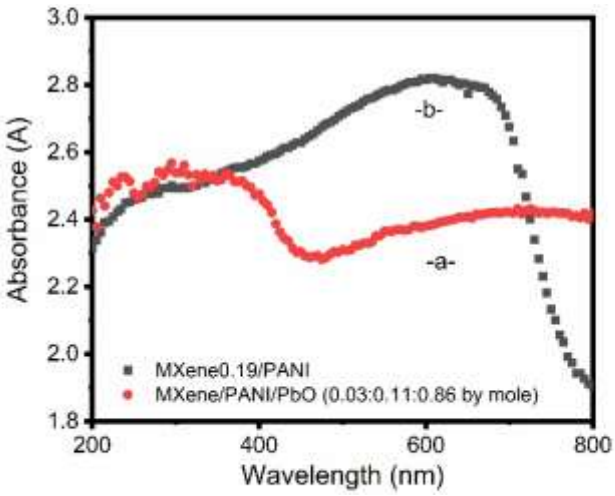

Fig. 2. Absorbance plots vs. wavelength for for a)MXene0.19:PANI b) MXene0.03/PbO0.86/PANI0.11 nanocomposite

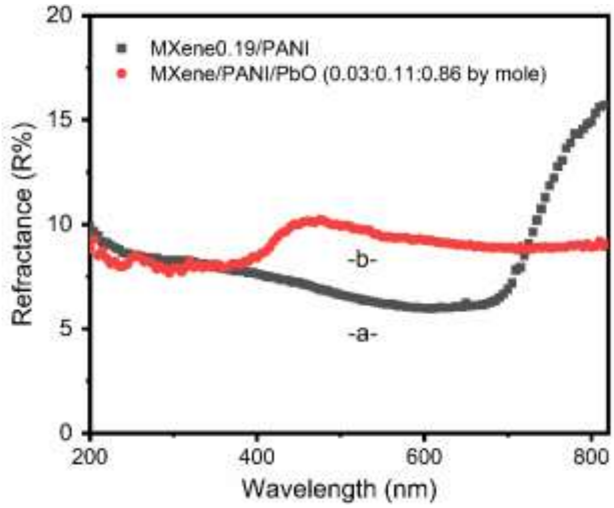

Fig. 3. Reflectance plots vs. wavelength for a)MXene0.19-PANI b) MXene0.03/PbO0.86/ PANI0.11 nanocomposite

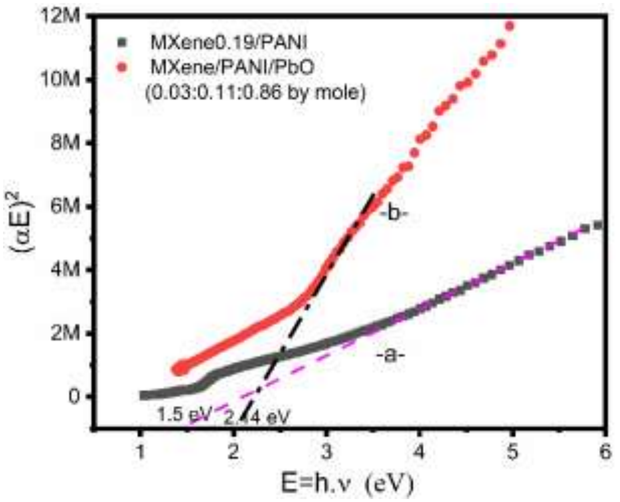

Fig. 4. Plots of $(\alpha h\upsilon)^2$ vs. photon energy for a) MXene0.19-PANI b) MXene0.03/PbO0.86/PANI0.11 nanocomposite

3.2. The refractive index and dielectric constants of the MXene based nanostructured thin film

The optical response of the MXene-based nanostructured thin film was characterized through its reflectance (R), refractive index (n), and the real (ε′) of the complex dielectric permittivity. Dispersion characteristics are critical in optical materials research due to their direct influence on photonic device performance, optical communication efficiency, and spectral-dispersion-based device engineering. Optical measurements were conducted over the 200–800 nm range under normal incidence using a UV–Vis system that simultaneously records absorbance (A) and reflectance (R). The wavelength-dependent refractive index profiles for MXene0.19–PANI and MXene0.03:PANI0.11:PbO0.86 nanocomposite are presented in Figs. 5a and 5b, respectively. Fig. 5a demonstrates that n decreases monotonically from ~1.90 to ~1.55 up to 700 nm, after which a rapid increase occurs, indicating a transition from normal to anomalous dispersion beyond 700 nm.

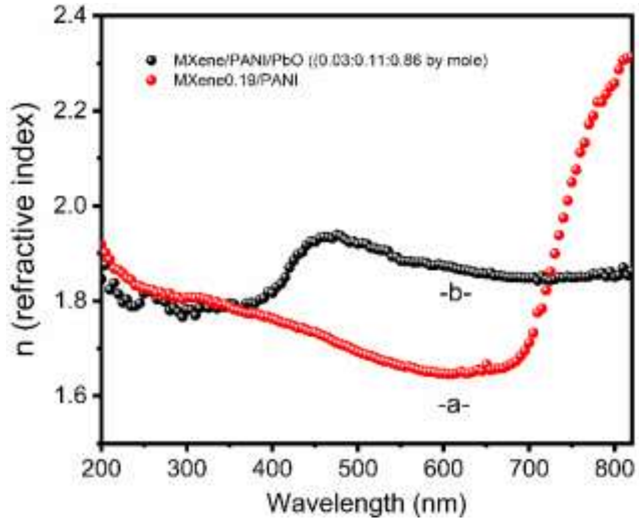

Fig. 5. The variation of refractive index for a)MXene0.19-PANI b) MXene0.03/PbO0.86/PANI0.11 nanocomposite

In Fig.5b, MXene0.03/PbO0.86/PANI0.11 nanocomposite exhibits an approximately constant n value (~1.8) versus the UV range, followed by a pronounced peak (~1.95) at 465 nm and a subsequent saturation for $\lambda > 600$ nm. The electronic excitation dynamics of the composites were analyzed through the complex dielectric function, expressed as $\varepsilon(\omega) = \varepsilon'(\omega) + i\,\varepsilon''(\omega)$. The real and imaginary components were derived from the refractive index (n) and extinction coefficient (k) using the standard relations provided in reference [25].

$$\varepsilon' = n^2 - k^2 \quad (2)$$
$$\varepsilon'' = 2nk \quad (3)$$

Fig. 6 illustrate the dependence of the ε′ vs. wavelength for MXene0.19:PANI and MXene0.03/PbO0.86/PANI0.11 nanocomposite. As shown in Fig. 6a the ε′ value of the MXene0.19:PANI nanocompo-site decrease with increasing wavelength from the UV region up to 700 nm in the visible region. The real and imaginary parts of the dielectric constant exhibit different behaviors. As seen in Fig. 6b, the dielectric constant of MXene0.19:PANI decreases up to 700 nm, whereas the MXene0.19:PANI nanocomposite displayed in Fig. 6b exhibits a relaxation behavior at 465 nm. In other words, the polarization of the composite increases with increasing wavelength in the 400–465 nm range. A similar behavior is also observed in the MXene0.03:PANI0.11: PbO0.86 nanocomposite.

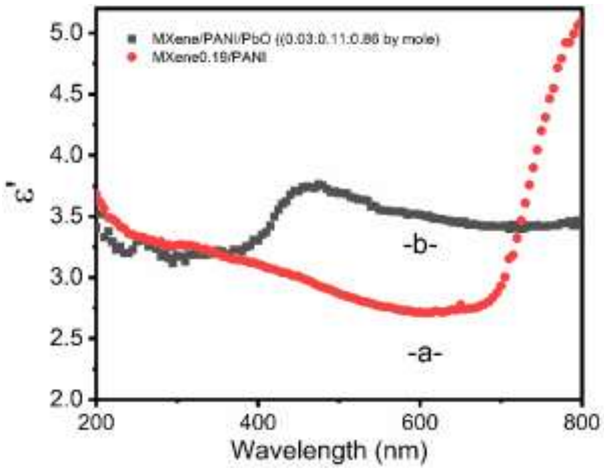

Fig. 6. The variation of real part of dielectric constant for a)MXene0.19:PANI b)MXene0.03/PbO0.86/PANI0.11 nanocomposite

Figs. 7a and 7b depict the optical conductivity spectra of the MXene0.19:PANI and MXene0.03/PbO0.86/PANI0.11 nanocomposites as a function of incident photon wavelength. Both samples exhibit comparable trends within the UV region. In Fig. 7b, a slight increase in optical conductivity is observed near 400 nm, followed by a monotonic decrease from approximately 445 nm to 800 nm. Conversely, the MXene0.19:PANI nanocomposite (Fig. 7a) shows a pronounced rise in optical conductivity beyond ~700 nm. This behavior may be attributed to the enhanced absorbance and reduced transmittance of the thin films in this spectral range, coupled with electron excitation processes driven by the decreasing photon energy. Moreover, the relatively higher PANI content in the MXene0.19:PANI composite likely contributes to a reduced optical band gap and an increased density of available energy states, thereby promoting higher optical conductivity [26].

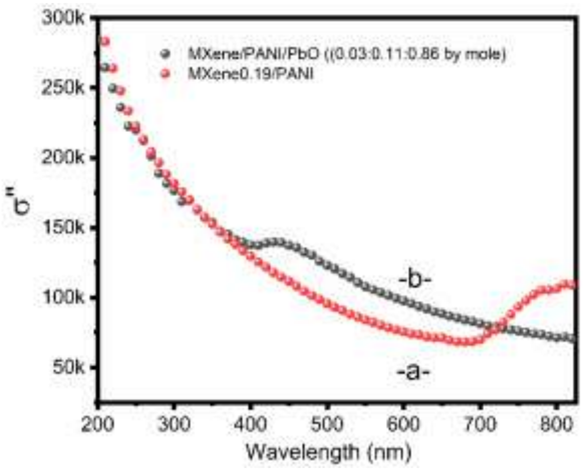

Fig. 7. The variation of conductivity for a) MXene0.19-PANI b) MXene0.03/PbO0.86/ PANI0.11 nanocomposite

4. Conclusion

The present study successfully demonstrates the synthesis of $Ti_3C_2T_x$ MXene from the Ti_3AlC_2 MAX phase through a wet chemical etching approach utilizing a mixture of hydrofluoric acid (HF). Structural characterization using SEM confirmed the formation of the $Ti_3C_2T_x$ phase. The optical band gap and optical constants (refractive index, reflectance, real parts of the complex dielectric constant) of MXene, PANI and PbO nanostructured composite systems were determined. The results, also, indicated that the changing in MXene content affected the optical bandgap, Urbach energy, refractive index, extinction coefficient, optical dielectric constant and optical conductivity of the nanocomposites. In this regards, it was determined the optoelectronic properties of MXene0.03/PANI0.11/ PbO0.86 nanocomposites with MXene and PANI. MXene with PANI matrix exhibited a narrowed band gap of 1.5 eV and improved interparticle connectivity. The band gap of MXene0.03/PANI0.11/PbO0.86 was also found to be 2.14 eV. All of these are important for enhancing charge transport and light-matter interaction.

References

[1] M. Boota, Y. Gogotsi, Adv. Energy Mater, MXene—conducting polymer asymmetric, Pseudocapacitors, 2018, 9, 1802917.

[2] F. Bu, M. M. Zagho, Y. Ibrahim, B. Ma, A. Elzatahry, D. Zhao, Porous MXenes: Synthesis, structures, and applications, Nano Today, 2020, 30, 100803.

[3] M.-S. Cao, Y.-Z. Cai, P. He, J.-C. Shu, W.-Q. Cao, J. Yuan, 2D MXenes:electromagnetic property for microwave absorption and electromagnetic interference shielding, Chem. Eng. J. 2019, 359, 1265.

[4] S.K. Pasha, K. Chidambaram, L.J. Kennedy, J.J. Vijaya, Lead oxide - PbO humidity sensor, Sens. Trasducers J., 122 (11) (2010), p. 113

[5]V.D. Araujo, M.R.B. Andreeta, L.J.Q. Maia, R.M. Nasci mento, F.V. Motta, M.R.D. BomiO, C.A. Paskocimas, M.I.B. Bernardi, V.D. Araujo, M.R.B. Andreeta, L.J. Q. Maia, R.MNascimento, F.V. Motta, M.R.D. Bomio , C.A. Paskocimas,M.I.B. Bernardi, Microstructural, structural and optical properties of nanoparticles of $PbO-CrO_3$ pigment synthesized with a soft route, Ceramica, 61 (2015), p. 118

[6]N.T. Sharma, V. Vaishampayan, R.K. Kaushal, Synthesis, characterization application of nano pno catalyst, Int. J. Nano. Mater Sci., 4 (1) (2015), p. 87

[7]A. Rajabi, M. Aieneravaie, V. Dorosti, S.K. Sadrnezhad, Development and biomedical application of nanocomposites: in situ fabrication of ZnO- PbO

nanocomposite through microwave method, Mater. Tech: Adv. Perf. Mater., 29 (4) (2016), p. 227

[8]S. Radhakrishnan, M.N. Kamalasanam, P.C. Mahendru, Sensitization of photoconductivity in tetragonal lead monoxide, J. Mater. Sci., 18 (1983), p. 1912

[9] G. Triniquer, R. Hoffman, Lead monoxide-electronic structure and bonding, J. Phys. Chem., 88 (1984), p. 6696

[10] A.A. Novruzova, M.A. Ramazanov, A. Chianese, V.F. Hajiyeva, A.M. Maharramov, U. A. Hasanova, Synthesis structure and optical properties of PP1PbS/CdS hybrid Nanocomposites, Chem. Eng. Trans. 60 (2017).

[11] U. Ali, K.J.B. Abd Karim, N.A. Buang, A review of the properties and applications of poly (methyl methacrylate) (PMMA), Polym. Rev. 55 (2015) 678 705.

[12] A. Badhe Rashmi, A. Ansari, S.S. Garje, Study of optical properties of TiO2 nanoparticles and CdS@TiO2 nanocomposites and their use for photocatalytic degradation of rhodamine B under natural light irradiation, Bull. Mater. Sci. 44 (2021) 1 11

[13] R. Kotsilkova, Thermoset nanocomposites for engineering applications, Smithers Rapra Technology Limited, UK, 2007, ISBN: 978-1-84735-062-6.

[14] K. Demirelli, C. Ercan, İ. Erol and F. Yakuphanoğlu, Dielectric response and Surface Wettability in Advanced MXene nanocomposites: Insights from contact Angle Measurements, Silicon, 2025 (submitted).

[15] Q. Ma, J. Wang, X. Dong, W. Yu, G. Liu, Adv. Funct. Mater. 2015, 25,2436.

[16] V. H. Nguyen, R. Tabassian, S. Oh, S. Nam, M. Mahato,P. Thangasamy, A. Rajabi-Abhari, W.-J. Hwang, A. K. Taseer, I.-K. Oh, Adv. Funct. Mater. 2020, 30, 1909504.

[17] Y. Xia, T. S. Mathis, M. Q. Zhao, B. Anasori, A. Dang, Z. Zhou,H. Cho, Y. Gogotsi, S. Yang, Nature 2018, 557, 409.

[18] Z. Fan, Y. Wang, Z. Xie, X. Xu, Y. Yuan, Z. Cheng, Y. Liu, Nanoscale 2018, 10, 9642.

[19] Y. Fang, Y. Zhang, K. Zhu, R. Lian, Y. Gao, J. Yin, K. Ye, K. Cheng, J. Yan, G. Wang, Y. Wei, D. Cao, ACS Nano 2019, 13,14319.

[20] S. Feng, Y. Yi, B. Chen, P. Deng, Z. Zhou, C. Lu, ACS Appl. Mater. Interfaces 2022, 14, 36060.

[21] V.N. Suryawanshi, Ashwini S. Varpe, Mrinalini D. Deshpande, Band gap engineering in PbO nanostructured thin films by Mn doping, Thin Solid Films 645 (2018) 87–92

[22] Z. Li, Z. Wang, W. Lu, B. Hou, Metals 2018, 8, 652.

[23] Z. Li, H. Zhang, J. Han, Y. Chen, H. Lin, T. Yang, Adv. Mater. 2018, 30, 1706981.

[24] Z. K. Li, Y. Wei, X. Gao, L. Ding, Z. Lu, J. Deng, X. Yang, J. Caro, H. Wang, Angew. Chem. Int. Ed. 2020, 59, 9751.

[25] J.N. Hodgson, Optical Absorption and Dispersion in Solids, Chapman and Hall Ltd.,11, New fetter Lane London EC4, 1970.

[26] S. Chala, M. Bdirina, · M. Elbar, · Y. Naoui, · Y. Benbouzid, T. Eddine T. M. Labed, · R. Boumaraf, · A.F. Bouhdjar, · N. Sengouga, · F. Yakuphanoğlu, S.Rahmane, Dependence of Structural and Optical Properties of ZnO Thin Films Grown by Sol–Gel Spin-Coating Technique on Solution Molarity, Transactions on Electrical and Electronic Materials (2022) 23:544–551